

## Luminescence of the $\text{Cr}^{3+}$ ion in sodium $\beta$ - and $\beta'$ -alumina: Site selection by time-resolved fluorescence line narrowing

F. Rossi and G. Mariotto

*Dipartimento di Fisica, Università di Trento, 38050 Povo (Trento), Italy*

M. Montagna

*Dipartimento di Fisica, Università di Trieste, Via Valerio 2, 34127 Trieste, Italy*

M. Ferrari

*Consiglio Nazionale delle Ricerche, Centro di Fisica degli Stati Aggregati ed Impianto Ionico, 38050 Povo (Trento), Italy*

(Received 17 May 1993)

Fluorescence of  $\text{Cr}^{3+}$  ions in the two different octahedral sites of the spinel block of  $\beta$ - and  $\beta'$ -alumina have been measured by time-resolved fluorescence line-narrowing spectroscopy. For the excitation either a pulsed or a chopped cw-dye laser was used. Lifetimes and splittings of the ground state ( ${}^4A_2$ ) and of the  ${}^2E$  state have been measured by tuning the excitation energy within the inhomogeneous profile of the  $R_1$  and  $R_2$  lines of the split  ${}^2E$ - ${}^4A_2$  transition. In sodium  $\beta'$ -alumina, we have isolated several inequivalent emitting centers, which are related to different configurations of the stabilizing  $\text{Mg}^{2+}$  ions.

### I. INTRODUCTION

Sodium  $\beta'$ -alumina is a well-known superionic compound which has been extensively studied as a prototype of solid electrolytes for Na/S battery applications.<sup>1</sup> During the last years it has increasingly stimulated optical investigations after the discovery that it is able to incorporate a large variety of divalent and trivalent transition-metal and rare-earth ions in the conduction region of its structure, via ion-exchange reactions.<sup>2,3</sup> The exchanged compositions show very rich optical spectra thus making the material a very promising candidate for optoelectronic applications. So, for instance, observations of laser action<sup>4</sup> and optical phase conjugation<sup>5</sup> in the  $\text{Nd}^{3+}$  substituted  $\beta'$ -alumina have been recently gained, and other very interesting optical effects have been reported in partially  $\text{Cu}^+$ -substituted compositions.<sup>6</sup>

In principle, through the ion-exchange technique, it becomes possible to prepare a lot of such compositions with controlled amounts of chromophors in dependence of the desired applications. This fact, of course, prompted increasing interest in probing the optical performances of such compound and their derivatives. However, besides the technological interest, the optical properties of  $\beta'$ -aluminas doped with transition-metal and rare-earth ions turn out very attractive also for fundamental studies.

Optical spectroscopy of solids provide important information for understanding the fundamental interactions between the luminescent ion and the host lattice, as well as the interactions between optically active ions, which are important mechanisms affecting the energy relaxation in solids. With this respect, the luminescent ions, incorporated via ion-exchange reactions in the conduction plane regions, constitute very reliable tools for probing the local structure as well as the energy relaxation in  $\beta'$ -aluminas, since their fluorescence spectra are very sensi-

tive to the disordered distribution and motion of the mobile ion sublattice. In particular, the temperature-activated diffusion of mobile ions in such systems may provide new degrees of freedom for energy relaxation: in fact, this nonradiative decay mechanism has been postulated to occur in  $\text{Cr}^{3+}$ -substituted  $\beta'$ -alumina.<sup>7,8</sup>

An alternative approach exploits the optical properties of impurity ions incorporated during the crystal growth process in the spinel block sites, where they suffer much less the effects of both the disordered distribution and the ion diffusion occurring in the conduction regions. In previous studies we have successfully used optical spectroscopy of  $\text{Cr}^{3+}$  in spinel block sites of sodium  $\beta$ -alumina to probe the local structure, as well as the disorder in the conduction plane regions. We have shown that by time-resolved spectroscopy it is possible to measure the contribution to the luminescence of centers in different crystal sites.<sup>9</sup> For all sites, the inhomogeneous linewidths of the emission lines are quite large, and the temperature dependence of their homogeneous linewidths shows a behavior similar to that observed in polymers and glasses.<sup>10</sup> The homogeneous broadening of the lines in these systems is believed to be mainly due to the interaction of the optically active ions with the two-level systems (TLS), originally introduced to explain the low-temperature anomalies observed in amorphous systems like glasses and polymers.<sup>11</sup> The TLS presence in  $\beta$ -aluminas has been clearly revealed by very low-temperature measurements of thermal, dielectric, and acoustic properties.<sup>12</sup> Despite the large variety of their dynamic manifestations, nevertheless the microscopic nature of such TLS's has not yet been established and further studies, in partially disordered compounds, seem to be very promising to this aim.

The present paper reports on the results of a detailed study of the site dependence of  $\text{Cr}^{3+}$  ion luminescence in

as-grown crystals of sodium  $\beta$ - and  $\beta'$ -alumina, Mg stabilized. The luminescence originates from the  ${}^2E-{}^4A_2$  transition of  $\text{Cr}^{3+}$  substitutional for  $\text{Al}^{3+}$  ions in the octahedral sites of spinel block. Measurements were carried out at low temperatures by exciting at different energies within the inhomogeneous profile. Both lifetimes and splittings of either the ground or the excited state for the different set of centers have been measured.

In Sec. II, the crystal structure of  $\beta$ -aluminas is described with special attention to the defect nature of their conduction regions and to the charge compensation mechanisms occurring for the different crystal forms. In Sec. III, the sample synthesis and the experimental procedures used for time-resolved spectroscopy (TRS) experiments are described. The experimental results of TRS and fluorescence line-narrowing (FLN) measurements on sodium  $\beta$ -alumina and  $\beta'$ -alumina (Mg stabilized) are presented in Sec. IV. In Sec. V, a discussion of the main results of our study is done in terms of disorder within the mobile cation sublattice and in terms of the local environment of a  $\text{Cr}^{3+}$  ion which depends on the charge compensation mechanisms for the different compositions. Finally, some concluding remarks about the role of defects on the spectroscopic features of optical emissions from impurity ions in solids are given in Sec. VI.

## II. CRYSTAL STRUCTURE OF SODIUM $\beta$ - AND $\beta'$ -ALUMINA

The  $\beta$ -alumina group of oxides ( $\beta$ - and  $\beta'$ -) are defect structures consisting of slabs of four close-packed oxygen layers interspersed by layers which have a low atom density and which contain the mobile sodium cations. The closed-packed oxide slabs, which show mineral spinel structure, accommodate  $\text{Al}^{3+}$  ions in both tetrahedral and octahedral sites.<sup>13,14</sup> There are two main subgroups of  $\beta$ -alumina, whose space structures differ in the stacking sequence of layers up the crystallographic  $c$  axis. The first subgroup ( $\beta\text{-Al}_2\text{O}_3$ ), which is stacked according to a twofold screw axis, contains a mirror plane through the layers of mobile cations (conduction planes), and results in hexagonal crystal symmetry (space group  $D_{6h}^4$ ,  $P6_3/mmc$ , No. 194).<sup>14</sup> The mobile cations are distributed over three different sites (BR,  $a$ -BR, and mO) of the conduction plane, with a relative occupation ratio which depends on the temperature.<sup>14</sup> Ionic diffusion occurs, through the interstitialcy mechanism,<sup>15</sup> extensively within these open planes perpendicular to the  $c$  axis, since closed-packed  $\text{Al}_2\text{O}_3$  structure prevents any significant ionic migration along the  $c$  axis.

Sodium  $\beta$ -alumina is a nonstoichiometric compound due to some soda excess present in the conduction plane, whose amount depends on the crystal growth conditions and methods.<sup>16,17</sup> Generally, authors refer to sodium  $\beta$ -alumina formula as to  $(\text{Na}_2\text{O})_{1+x}\text{Al}_2\text{O}_3$ , where  $x$  accounts for the nonstoichiometry degree and typically ranges between 0.1 and 0.3. For the composition  $(\text{Na}_2\text{O})_{1.23}\text{Al}_2\text{O}_3$ , a suggestive picture of  $\text{Na}^+$ -ion distribution at 78 K has been obtained through the refinement neutron-diffraction data by Roth *et al.*<sup>18</sup> They locate 64% of  $\text{Na}^+$  ions in Beavers-Ross (BR) sites,

while the remaining fraction of  $\text{Na}^+$  ions shares in pairs mid-oxygen (mO) sites, thus making about 22% of conduction plane cells double occupied by sodium ions. Extra oxygen ions also locate in mO sites of these doubly occupied cells, where they bridge a couple of slightly displaced Al(1) ions of spinel blocks adjacent to the mirror plane. The resulting  $\text{Al}_v(1)\text{-Al}_i(3)\text{-O}_i(5)\text{-Al}_i(3)\text{-Al}_v(1)$  complex is usually referred as to a double Frenkel defect.<sup>18</sup>

The  $\beta'$ -alumina subgroup is stacked according to the threefold screw axis, contains no mirror plane, and has rhombohedral symmetry (space group  $D_{3d}^5$ ,  $R\bar{3}m$ , No. 166).<sup>13</sup> Its unit cell is 50% larger than that of  $\beta$ -alumina because of the difference in the stacking sequence. Adjacent close-packed slabs are held apart by Al-O-Al spacer units, but in this structure the sodium atom sites lie above and below the plane through the center of the oxide spacer atoms and the  $\text{Na}^+$ -ion diffusion path encompasses a finite volume (the conduction slab) rather than a plane as in the  $\beta$ -alumina structure. The projected three-dimensional view of the  $\beta'$ -alumina structure, i.e., of the region saddling the conduction plane region, plotted in Fig. 1 clearly shows the layered character of this material, which consists of close-packed spinel-like blocks of  $\text{Al}_2\text{O}_3$  alternating low-density stacking regions (conduction planes).

Sodium  $\beta'$ -alumina is a ternary system, usually stabilized by addition of spinel-forming cations, as  $\text{Mg}^{2+}$  or  $\text{Li}^+$ , which replace a proper fraction of  $\text{Al}^{3+}$  ions, prefer-

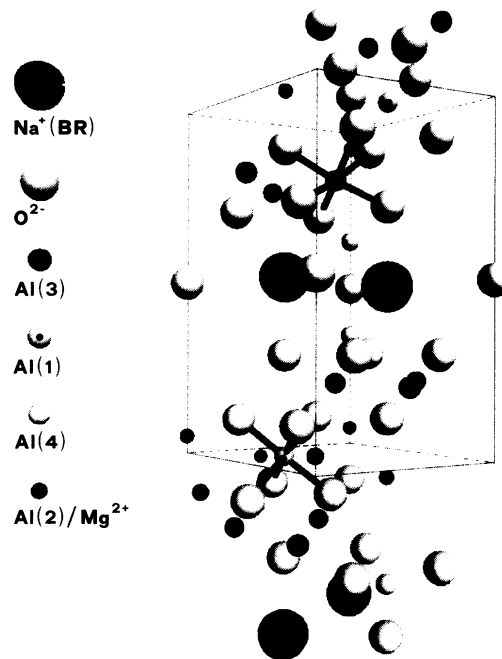


FIG. 1. Stereoscopic view of sodium  $\beta'$ -alumina structure, showing two half spinel blocks adjacent to the conduction plane region. The tetrahedral and octahedral sites of  $\text{Al}^{3+}$  ions within the spinel block are labeled according to Ref. 20. The ligands of the two octahedral sites are evidenced.  $\text{Na}^+$  ions are located in Beavers-Ross (BR) sites, but slightly displaced ( $\approx 0.17$  Å) out from the plane of the bridging oxygens O(5). Finally, the stabilizing  $\text{Mg}^{2+}$  ions are substitutional for  $\text{Al}^{3+}$  ions in Al(2) sites.

entially at the Al(2) tetrahedral sites.<sup>18,19</sup> Mg-stabilized compounds have the general formula  $\text{Na}_{1+x}\text{Mg}_x\text{Al}_{11-x}\text{O}_{17}$ . The most studied specimen is  $\text{Na}_{1.67}\text{Mg}_{0.67}\text{Al}_{10.33}\text{O}_{17}$ . Due to the substoichiometric sodium content, some sites in the conduction plane are vacant and, therefore,  $\text{Na}^+$ -ion diffusion in  $\beta'$ -alumina occurs via a vacancy mechanism. Besides the mechanical disorder of  $\text{Na}^+$  ions in the conduction region, this compound also presents some degree of chemical disorder inside the spinel block, due to the stabilizing divalent cations at the tetrahedral  $\text{Al}^{3+}$  sites.<sup>18</sup>

Within the spinel block of  $\beta$ - and  $\beta'$ -alumina there are two inequivalent octahedral sites available for substitution of the  $\text{Al}^{3+}$  ion by the  $\text{Cr}^{3+}$  ion (see Fig. 1 for a projected view of the neighborhood of the two sites within the spinel block).<sup>18</sup> The site at the middle of the spinel block, referred as to site Al(4) in the  $\beta$  phase<sup>14</sup> and site Al(1) in the  $\beta'$  phase,<sup>20</sup> respectively, has inversion symmetry (site group  $D_{3d}$ ). The second octahedral site [site Al(1) in  $\beta$ -alumina<sup>14</sup> and site Al(3) in  $\beta'$ -alumina<sup>20</sup>], is located closer to the conduction region and shows a lower degree of symmetry (site group  $C_3$ ).

### III. CRYSTAL GROWTH. EXPERIMENTAL PROCEDURES

Single crystals of melt-grown sodium  $\beta$ -alumina were originally supplied by Union Carbide Co. in the non-stoichiometric  $(\text{Na}_2\text{O})_{1.23}11\text{Al}_2\text{O}_3$  composition. The samples used in our experiments were cut from a larger boule in regular platelets with typical dimensions of  $8 \times 5 \times 0.5$  mm<sup>3</sup>. They showed very high optical quality, being completely transparent and without any appreciable surface damage.

Sodium  $\beta'$ -alumina crystals, Mg stabilized, were grown at 1675 °C from a melt of  $\text{Na}_2\text{O}$ ,  $\text{MgO}$ , and  $\text{Al}_2\text{O}_3$  by a flux evaporation method, as reported by Briant and Farrington.<sup>21</sup> They were cut in quite small platelets (typical size  $4 \times 4 \times 0.2$  mm<sup>3</sup>) of nominal composition  $\text{Na}_{1.67}\text{Mg}_{0.67}\text{Al}_{10.33}\text{O}_{17}$ .

Both these compositions contain traces of  $\text{Cr}^{3+}$  ions, incorporated as natural impurities of  $\text{Al}^{3+}$  ions in spinel block sites during the crystal growth. In sodium  $\beta'$ -alumina crystals trace amounts of  $\text{Mn}^{2+}$  ion were also detected.<sup>22</sup>

A different set of Mg-stabilized sodium  $\beta'$ -alumina crystals, doped with a controlled (5000 ppm) amount of  $\text{Cr}_2\text{O}_3$ , was provided by Airtron Co. These samples looked slightly red in color, due to the  $\text{Cr}^{3+}$  doping.

Finally, some small (typical size  $4 \times 3 \times 0.5$  mm<sup>3</sup>) single crystals of Na  $\beta$ -alumina, intentionally doped with  $\text{Cr}^{3+}$  ions, were grown by us from a molten flux of  $\text{Bi}_2\text{O}_3$  following the procedure used by McWhan *et al.*<sup>17</sup> The crystals were optically clear and transparent, although they nominally contained about 500 ppm of  $\text{Cr}^{3+}$  ions.

Before the measurements our  $\beta$ - and  $\beta'$ -alumina crystals underwent prolonged thermal treatment in an inert atmosphere at 420 and 450 °C, respectively, in order to get a satisfactory dehydration. During the experiments they were mounted into an optical cryostat kept under the vacuum of a diffusion pump.

The excitation spectra were obtained under irradiation

of a tungsten lamp filtered by a single monochromator, with a spectral resolution of about 20 cm<sup>-1</sup>, while the emission spectra were obtained under excitation of the 514.5-nm line of a cw  $\text{Ar}^+$ -ion laser. A pulsed dye laser (linewidth of 0.2 cm<sup>-1</sup>), pumped by an excimer laser, and a ring dye laser (linewidth of 0.1 cm<sup>-1</sup>) pumped by an  $\text{Ar}^+$ -ion laser were used for site-selective excitation experiments. The light beam was focused on the sample by a 25 cm focal length lens. The luminescence was analyzed by a 0.8-m focal length double monochromator with a resolution limit of 0.15 cm<sup>-1</sup>, and detected by a standard photon-counting system, interfaced to a personal computer.

Light pulses of variable duration between 1 and 50 ms were produced by focusing the filtered light of the lamp or the cw laser beam on a chopper wheel. The wheel shape and the chopper speed were chosen in order to match the temporal response of our samples. The reference output of the chopper triggered either the scans of the multichannel analyzer in decay-time measurements or some temporal windows of detection in the time-resolved experiments, allowing the simultaneous detection of spectra at different delays.

### IV. RESULTS

#### A. General features of $\text{Cr}^{3+}$ -ion fluorescence in $\beta$ - and $\beta'$ -alumina

The luminescence spectra obtained at 77 K under cw excitation of the 514.5-nm line from Na  $\beta$ -alumina and Na  $\beta'$ -alumina, Mg stabilized, are reported in Figs. 2(a) and 2(b), respectively. Both spectra show a rather complex structure, with several bands of different width. Nonexponential decays are observed at any frequency in lifetime measurements on both samples. This indicates that optically active ions are located in inequivalent sites. Site selection can be achieved in different ways: in fact, the shape of the luminescence in time-resolved spectra depends on the frequency, polarization, and pulse width

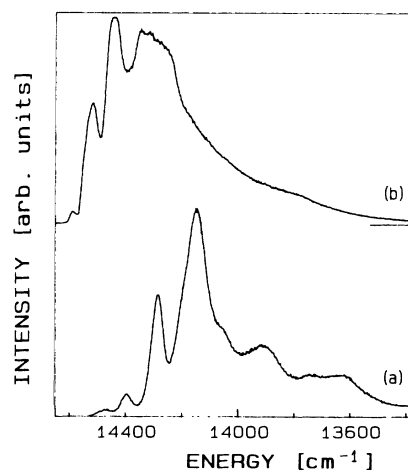


FIG. 2. Luminescence spectra of  $\text{Cr}^{3+}$  ion, obtained in (c,c) polarization at 77 K under continuous excitation of the 514.5-nm line: (a) sodium  $\beta$ -alumina; (b) sodium  $\beta'$ -alumina, Mg stabilized.

of the exciting light, as well as on the polarization of emitted light and delay of detection. Two main contributions to the luminescence were isolated by means of TRS measurements and assigned to the  ${}^2E-{}^4A_2$  transition of the  $\text{Cr}^{3+}$  ion in the two inequivalent octahedral sites of the  $\beta$  and  $\beta''$  structures.<sup>9,23</sup> The luminescence spectra from long-living centers ( $20 < \tau < 70$  ms), shown in Fig. 3, are assigned to  $\text{Cr}^{3+}$  in the site with inversion symmetry at the middle of spinel block, Al(4) in  $\beta$ -alumina and Al(1) in  $\beta''$ -alumina. On the contrary, the emissions from centers with lifetimes of few ms, reported in Fig. 4, are associated to  $\text{Cr}^{3+}$  ions in the octahedral site with  $C_S$  symmetry, Al(1) in  $\beta$ -alumina and Al(3) in  $\beta''$ -alumina.

The luminescence spectrum of long-living centers in  $\beta$ -alumina, recorded at 4.2 K [Fig. 3(a)], shows a zero-phonon line (ZPL) at  $14\,265\text{ cm}^{-1}$  with a full width at half maximum (FWHM) of about  $40\text{ cm}^{-1}$ , and a structured vibronic sideband (SB) on the low-energy side. In  $\beta''$ -alumina [Fig. 3(b)] the ZPL appears shifted to higher frequencies and splitted in three bands which seem to hide further internal structures.

Lifetime measurements performed at different wavelengths in  $\beta$ -alumina present a fast decay in the first few ms and a long tail, which can be well fit by a single exponential giving a lifetime of about 70 ms. If we set time delays greater than 20 ms in order to completely cut the contributions of short-lifetime centers, the spectra are independent from the delay. Therefore, the luminescence of Fig. 3(a) is characterized by a lifetime of 70 ms. The same measurements on  $\beta''$ -alumina show that only for some wavelengths the time decay pattern can be fitted by a single exponential even in the long delay tail. In general, at least two lifetimes are necessary to reasonably fit the long delay data, indicating that the observed luminescence originates from different sites. In fact, lifetime values ranging between 20 and 65 ms are observed and the actual shape of the spectrum sensitively depends on the time setup.

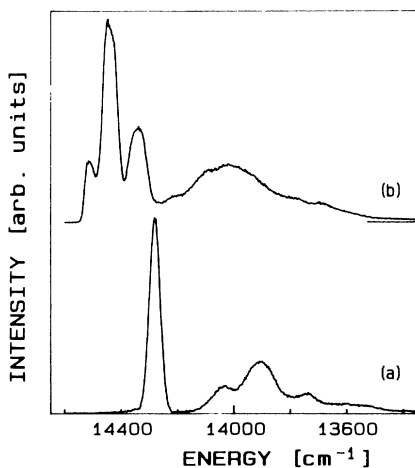


FIG. 3. Time-resolved luminescence spectra of  $\text{Cr}^{3+}$  ions at 4.2 K in (a) Na  $\beta$ -alumina and (b) Na  $\beta''$ -alumina: (a) pulse duration 50 ms and detection from 40 to 90 ms after laser switchoff; (b) pulse duration 40 ms and detection from 30 to 80 ms after laser switchoff.

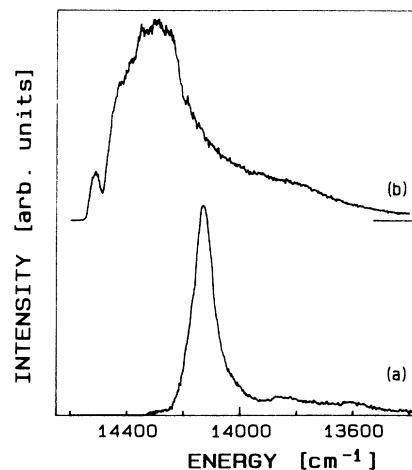


FIG. 4. Time-resolved luminescence spectra of  $\text{Cr}^{3+}$  ions in (a) Na  $\beta$ -alumina and (b) Na  $\beta''$ -alumina obtained at 4.2 K under excitation at 514.5 nm. Pulse duration (a) 4 ms and (b) 3 ms with simultaneous detection.

The spectra originated by short-living centers are characterized by larger inhomogeneous linewidths. In  $\beta$ -alumina [Fig. 4(a)] a single band, centered at  $14\,100\text{ cm}^{-1}$  with a FWHM of about  $100\text{ cm}^{-1}$ , is observed, while in  $\beta''$ -alumina the spectral range of ZPL's spans more than  $300\text{ cm}^{-1}$ . In both the spectra, due to the large inhomogeneous broadening, ZPL's and SB's are not well separated and FLN experiments have been performed in order to isolate the respective contributions. Moreover, several lifetimes, in the range between 1 and 7 ms, are observed in the full spectra of both compositions, so that their shape strongly depends on the time setup, especially for  $\beta''$ -alumina where the spread in the decay times is greater.

The strength of the crystal field at the impurity site can be obtained from excitation spectra. Typical excitation spectra of  $\text{Cr}^{3+}$  in Na  $\beta''$ -alumina are shown in Fig. 5. The two bands, centered at about 550 and 400 nm, are due to the spin-allowed  ${}^4A_2-{}^4T_2$  and  ${}^4A_2-{}^4T_1$  transitions of  $\text{Cr}^{3+}$  ions in octahedral sites. The crystal-field parameter  $Dq$ , deduced from the energy of the  ${}^4A_2-{}^4T_2$  transition, is  $1720$  and  $1930\text{ cm}^{-1}$  for the centers with shorter and longer lifetimes, respectively [Figs. 5(b) and 5(c)]. In a crystal field lower than cubic the two quartets should be split, but possible internal structures of the bands are not resolved in the spectra of Fig. 5. In the spectrum of Fig. 5(c) a weak structure is present at  $15\,125\text{ cm}^{-1}$ . It has to be assigned to the  ${}^4A_2-{}^2T_1$  transition, but even in this case the expected internal structures, due to the spin-orbit interaction and trigonal field, are not observed. The spectra of Fig. 5 are taken by detecting at  $14\,320\text{ cm}^{-1}$  at the lowest-energy peak of ZPL structure of Fig. 3(b). Excitation spectra taken at different detection energies are very similar: the large homogeneous widths of the  ${}^4A_2-{}^4T_2$  and  ${}^4A_2-{}^4T_1$  bands tend to hide the inhomogeneous effects. The time-resolved excitation spectra of  $\beta$ -alumina do not present important differences from those of  $\beta''$ -alumina.

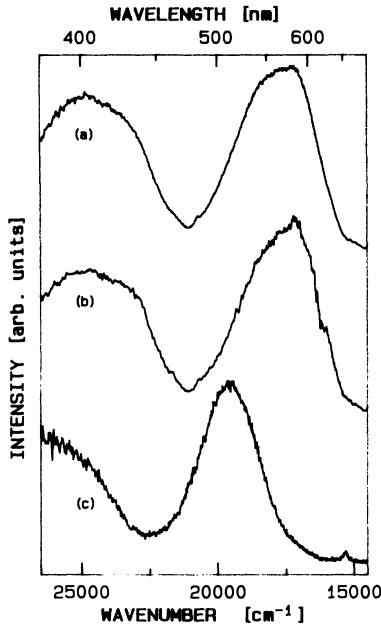


FIG. 5. Time-resolved excitation spectra of a  $\text{Cr}^{3+}$  ion recorded at 77 K in Na  $\beta'$ -alumina, for emissions observed at  $14\,320\text{ cm}^{-1}$ : (a) continuous excitation; (b) pulse duration 5 ms with simultaneous detection; (c) pulse duration 60 ms and detection from 20 to 70 ms after laser switchoff.

### B. Sodium $\beta$ -alumina

The luminescence spectra of Na  $\beta$ -alumina present a simpler structure with the respect of  $\beta'$  isomorph. At 4.2 K the luminescence with long lifetimes ( $\tau=70$  ms) consists of a broad ZPL ( $R_1$  line) and its sideband. At higher temperature a second line ( $R_2$ ) appears at higher energy ( $\Delta E=113\text{ cm}^{-1}$ ) and the lifetimes decrease (62 ms at 77 K, 44 ms at 300 K). The intensity ratio of the two lines has a temperature behavior which is well fitted by the equation  $I_{R_2}/I_{R_1} \approx \exp(-\Delta E/k_B T)$ , indicating thermal equilibrium between the population of the two Kramers doublets of the  ${}^2E$  split state.

The intensity ratio of the two lines, at a given temperature, depends on the polarization of the luminescence. Figure 6 shows the room-temperature luminescence spectra from long-living centers in different polarizations. The spectra were collected in the  $90^\circ$  geometries:  $a'(c,a')a$  [Fig. 6(a)],  $a'(c,c)a$  [Fig. 6(b)], and  $a'(a,a)c$  [Fig. 6(c)], with the usual notation for a scattering experiment, i.e., direction of incident laser beam (polarization of incident beam, polarization of emitted light) direction of emitted light. The two unoriented orthogonal directions in the mirror plane are labeled with  $a$  and  $a'$ , while  $c$  is the direction normal to the plane.

The shape of the spectra depends on the polarization of the emitted light, while the intensities depend also from the polarization of incidence and from the scattering geometry. The spectra in Figs. 6(a) and 6(b), recorded for the same sample orientation, differ only for the detection polarization and are indeed directly comparable. Spectrum 6(c) was obtained in a different geometry; its intensity was scaled to that of Fig. 6(a), in order to give the same intensity on the sidebands, which have more or less

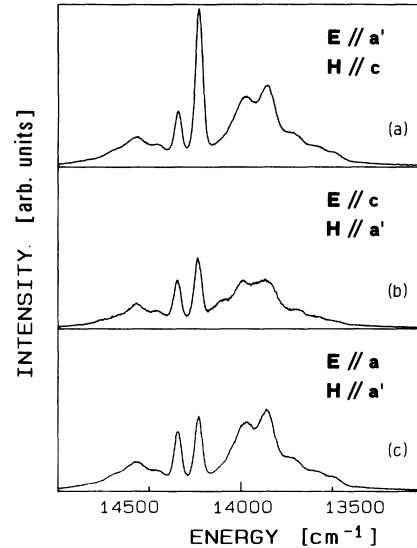


FIG. 6. Time-resolved luminescence spectra of  $\text{Cr}^{3+}$  ions in Na  $\beta$ -alumina obtained at 300 K, under excitation at  $514.5\text{ nm}$ , in different polarization settings: (a)  $a'(c,a')a$ ; (b)  $a'(c,c)a$ ; (c)  $a'(a,a)c$ . The directions of the electric and magnetic fields of the emitted light are reported. Pulse duration 40 ms and detection from 25 to 50 ms after laser switchoff.

the same shape. This normalization procedure is based on the assumption that the sideband is of pure electric-dipole (ED) character, and, therefore, its intensity depends only from the direction of the electric field of the emitted light. A comparison of the three spectra shows that the ZPL's have mainly magnetic-dipole (MD) character because their intensity is much more sensitive to the magnetic- than the electric-field direction of the emitted light.

For a more quantitative analysis of the results of Fig. 6, the intensity ratios of the lines in the different polarizations are reported in Table I. The intensities of the  $R_2$  lines was multiplied for the factor  $\exp(+\Delta E/k_B T)$ , in order to take into account the lower thermal populations of the upper doublet of the  ${}^2E$  state. Finally, the values are normalized to that of the  $R_1$  line in  $\mathbf{H}||c$  polarization.

Table I also reports the values of MD intensities calculated taking into account the spin-orbit (s.o.) coupling between the  ${}^2E$  and  ${}^4T_2$  states in trigonal symmetry. In a perturbative approach, the MD transition probabilities between the  $|{}^4A_2m_s^a\rangle$  ground-state sublevel and the excited  $|{}^2E\gamma^e m_s^e\rangle$  state, is proportional to the following expression:

TABLE I. Relative transition probabilities for  $R_1$  and  $R_2$  components of the  ${}^2E \rightarrow {}^4A_2$  transition as obtained from the data of Fig. 6. The calculated MD transition probabilities in trigonal symmetry are also reported (see text).

Pol.	$R_1$		$R_2$	
	Expt.	(Calc. DM)	Expt.	(Calc. DM)
$\mathbf{E}  c, \mathbf{H}  a'$	0.4	$0.5 \cdot \Delta$	0.49	$0.83 \cdot \Delta$
$\mathbf{E}  a, \mathbf{H}  c$	1	1	0.5	0.33
$\mathbf{E}  a, \mathbf{H}  a'$	0.44	$0.5 \cdot \Delta$	0.55	$0.83 \cdot \Delta$

$$|\langle {}^4A_2 m_s^a | M_q | {}^2E \gamma^e m_s^c \rangle|^2 = \left| \sum_{\gamma^t m_s^t} \frac{\langle {}^4A_2 m_s^a | M_q | {}^4T_2 \gamma^t m_s^t \rangle \langle {}^4T_2 \gamma^t m_s^t | H_{s.o.} | {}^2E \gamma^e m_s^c \rangle}{E({}^4T_2 \gamma^t m_s^t) - E({}^2E \gamma^e m_s^c)} \right|^2, \quad (1)$$

where  $M_q$  is the  $q$  component of the MD operator;  $\gamma^e$  and  $\gamma^t$  are the orbital components of  ${}^2E$ ,  ${}^4T_2$  states in trigonal symmetry;  $m_s^a$ ,  $m_s^e$ , and  $m_s^t$  are the spin components.

Notice that the transition probabilities depend on the energy difference between the two states coupled by the spin-orbit operator  $H_{s.o.}$ . In trigonal symmetry the orbital part of the  $T_2$  state splits into a doublet  $E(x_{\pm})$  and a singlet  $A(x_0)$ , the further splitting due to  $H_{s.o.}$  being negligible for important trigonal fields. The  ${}^2E$  state splits into two doublets:  $2A(u_{+1/2}^+, u_{-1/2}^-)$  and  $E(u_{-1/2}^+, u_{+1/2}^-)$ . Since

$$\langle {}^4A_2 m_s^2 | M_q | {}^4T_2 \gamma^t m_s^t \rangle = \langle {}^4M_2 | M | {}^4T_2 \rangle \delta_{m_s^a, m_s^t} \delta_{q, \gamma^t}, \quad (2)$$

transitions with  $\mathbf{H} \parallel \mathbf{c}$  ( $q=0$ ) are allowed to the  $x_0$  ( $\gamma^t=0$ ) state and transitions with  $\mathbf{H} \perp \mathbf{c}$  ( $q=\pm 1$ ) are allowed to the  $x_+$ ,  $x_-$  states. Different values for the energy gap appear in Eq. (1) if the  ${}^4T_2$  state is splitted by the trigonal field. The  $\Delta$  factor in Table I accounts for this effect and is given by

$$\Delta = \left| \frac{E({}^4T_2 x_0) - E({}^2E)}{E({}^4T_2 x_{\pm}) - E({}^2E)} \right|^2. \quad (3)$$

In Eqs. (1) and (3) the small  ${}^2E$  splitting ( $\Delta E \approx 113 \text{ cm}^{-1}$ ) is neglected.

The overall best agreement between the experimental and calculated MD transition probabilities is achieved for  $\Delta=0.7-0.8$ , i.e., with the  $E(x_{\pm})$  state at a higher energy than the  $A(x_0)$  state. The effects of the trigonal crystal field are described by the parameters  $v, v'$ .<sup>24</sup> The  ${}^4T_2$  splitting is given by

$$E({}^4T_2 x_0) - E({}^4T_2 x_{\pm}) \approx v/2, \quad (4)$$

being almost independent of  $v'$ . The  ${}^4A_2$  and  ${}^2E$  splittings are complicated functions of  $v, v'$  and of the spin-orbit parameters  $\xi, \xi'$  since many perturbative terms give important contributions.<sup>25,26</sup> In accordance to the method developed in Ref. 26, assuming  $Dq=1930 \text{ cm}^{-1}$  from the excitation spectra of Fig. 5(a), and taking for the other parameters those proper for ruby ( $B=650 \text{ cm}^{-1}$ ,  $C=3120 \text{ cm}^{-1}$ ,  $\xi=238 \text{ cm}^{-1}$ ,  $\xi'=199 \text{ cm}^{-1}$ ) the observed splittings of the  ${}^2E$  and  ${}^4A_2$  states (113 and  $0.1 \text{ cm}^{-1}$ , respectively, as we will see later) are reproduced by  $v=1900 \text{ cm}^{-1}$  and  $v'=250 \text{ cm}^{-1}$ . From Eq. (4) we would obtain a splitting of the  ${}^4T_2$  state of  $v/2 \approx 950 \text{ cm}^{-1}$ , the  $x_{\pm}$  sublevels being at a lower energy with respect to the  $x_0$  one. This, in turn, would give  $\Delta \approx 1.3$ , a value which lowers the agreement between observed and MD calculated intensities of Table I.

It should be noticed that the  ${}^4A_2 \rightarrow {}^4T_2$  band does not appear to be split in the excitation spectra. On the other hand, most of the intensity of the band is expected to be of ED character as it occurs for the  ${}^4A_2 \rightarrow {}^2E$ , due to the coupling with the odd vibrations. This fact could possi-

bly hide the splitting because in trigonal symmetry ED transitions to  $x_{\pm}$  are expected to be much more intense than to the  $x_0$  state, as observed, for example, in ruby. Alternatively, it is possible that the actual value of  $v$  is much lower than the exhibited one on the basis of the  ${}^2E$  splittings. In fact, in many systems the perturbative approach for the calculation of a large  ${}^2E$  splitting was found to fail.<sup>27,28</sup>

In conclusion, our results indicate that most of the  ${}^4A_2 \rightarrow {}^2E$  ZPL transition probability is of MD character, but only a partial agreement is obtained for the intensities calculated in a perturbative approach. Furthermore, the lack of observation of the splitting of the  ${}^4A_2 \rightarrow {}^4T_2$  band does not allow a definite determination of the parameters  $v$  and  $v'$  which describe the effect of the trigonal field.

The ratio  $R = I_{SB}/I_{ZPL}$  of SB to ZPL intensities, obtained at 77 K, where the different contributions are easily separated, are about 2 and 3 in the geometry of Figs. 6(a) and 6(b), respectively. This result is in agreement with the assignment of MD nature to ZPL and of ED to SB. In fact, the  ${}^2E \rightarrow {}^4A_2$  transition is weakly coupled to vibrations so that most of its intensity usually occurs in the ZPL lines (for instance, in ruby  $R=0.2$  in Elc).<sup>29</sup> However, when the ZPL is ED forbidden, a relatively strong sideband is observed due to parity mixing induced by odd vibrations ( $R=2$  in MgO).<sup>30</sup> Also the observed lifetime of 70 ms is indicative of an ED forbidden transition. A direct comparison can be made with ruby where the transition is ED allowed by the low symmetry of the crystal field ( $\tau=3.4 \text{ ms}$ ). In fact, the spin-forbidden  ${}^2E \rightarrow {}^4A_2$  transition gains intensity mainly by spin-orbit mixing of the  ${}^2E$  state with the  ${}^4T_2$  state, so that its oscillator strength is proportional to the square of inverse of the  ${}^4T_2 \leftrightarrow {}^2E$  energy separation [see Eq. (1)]. The excitation spectra show that the energy separation in  $\beta$ -aluminas is more or less the same as in ruby. Therefore, the much longer lifetime with respect to ruby must be attributed to a smaller oscillator strength of the  ${}^4A_2 \rightarrow {}^4T_2$  spin-allowed transition of the  $\text{Cr}^{3+}$  ion in a site with low distortion from the ideal  $D_{3d}$  symmetry, which does not allow ED transitions.

At 4.2 K, where the homogeneous broadening of the lines is negligible, the  $R_1$  line has a nearly Gaussian shape with a FWHM of  $40 \text{ cm}^{-1}$ . By narrow laser excitation inside the inhomogeneous profile the line is narrowed to the experimental resolution ( $0.2 \text{ cm}^{-1}$ ). Figure 7 shows FLN spectra obtained exciting in the  $R_1$  line at  $T=115 \text{ K}$ . At this temperature the homogeneous linewidth is not negligible, and the resonant luminescence has a distorted Lorentzian-like shape, with a pronounced tail toward the center of the inhomogeneous profile when the excitation occurs in the wings of the emission line. The line shape originates from the sum of spectra of different centers excited by the narrow laser band. Assuming that each center emits in a Lorentzian  $L$  of width

$\Gamma'$  centered at its mean frequency transition  $\nu'$ , we have for the luminescence line shape  $I(\nu)^{31}$

$$I(\nu) \approx \int N(\nu') L(\nu - \nu', \Gamma') d\nu' . \quad (5)$$

The distribution of the excited sites  $N(\nu')$  is given by

$$N(\nu') \approx L(\nu' - \nu_L, \Gamma') G(\nu') , \quad (6)$$

where  $G(\nu')$  is the density of sites having the transition at  $\nu'$  (i.e., the inhomogeneous profile of the absorption line), and

$$L(\nu' - \nu_L, \Gamma') = (\Gamma/2\pi) / [(\nu' - \nu_L)^2 + (\Gamma/2)^2]$$

gives the probability of exciting at  $\nu_L$  a site having the transition centered at  $\nu'$ .

The experimental curves were fitted in the free parameter  $\Gamma'$  by using Eqs. (5) and (6) and taking for  $G(\nu')$  a Gaussian centered at  $14260 \text{ cm}^{-1}$  with  $\text{FWHM} = 40 \text{ cm}^{-1}$ . With these values we fit quite well the low-temperature inhomogeneous profile, apart for a little thermal shift (at 4.2 K the line is centered at  $14265 \text{ cm}^{-1}$ ). The fits give  $\Gamma' = 6 \text{ cm}^{-1}$  for all the excitation energies in the inhomogeneous profile: the crystal-field inhomogeneities do not affect very much the coupling of

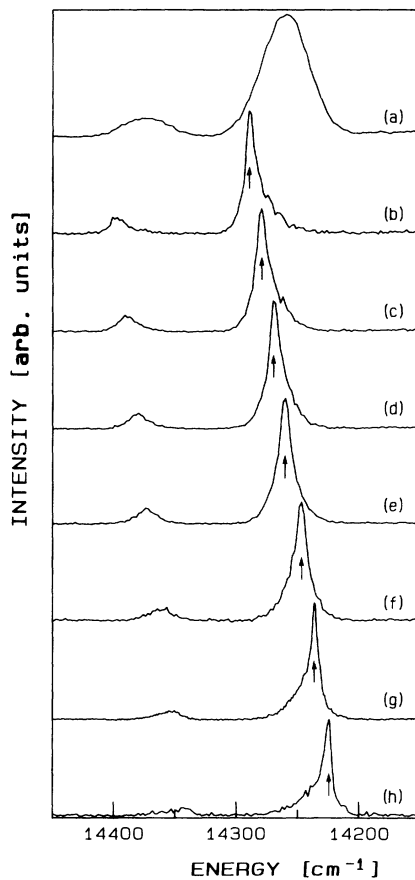


FIG. 7. Time-resolved luminescence spectra of  $\text{Cr}^{3+}$  ions in Na  $\beta$ -alumina obtained at 115 K in  $(c,c)$  polarization. Pulse duration 50 ms and detection from 30 to 80 ms after laser switchoff. (a) Inhomogeneous profile of ZPL obtained under excitation of the 514.5-nm line in the  ${}^4A_2\text{-}{}^4T_2$  band, (b)–(h) excitation energy set by the arrow.

the ion with the vibrational dynamics of the host system.

Figure 7 shows that the thermally excited luminescence in the  $R_2$  line is also narrowed. The  $R_1$ – $R_2$  splitting remains constant at  $113 \text{ cm}^{-1}$  by changing the excitation energy across the  $R_1$  line.

The inhomogeneous linewidth presents a value ( $40 \text{ cm}^{-1}$ ) intermediate between that observed in crystals (of the order of  $1 \text{ cm}^{-1}$ ) and in glasses (hundreds of  $\text{cm}^{-1}$ ): the mirror plane structure is highly defective like a glass but the Al(4) site, at the middle of the spinel block, has a short-range crystalline environment.

The poor resolution of our apparatus ( $\sim 0.2 \text{ cm}^{-1}$ ) and the weakness of the signal do not permit resolution of the expected low-temperature three-peaked structure due to the ground-state splitting (GSS). The GSS in the Ag  $\beta$ -alumina sample, doped with 1000 ppm of  $\text{Cr}^{3+}$ , was found by extrapolating to zero field the data from FLN measurements under magnetic fields along the  $c$ -axis direction up to 5 T. The  ${}^4A_2(\pm\frac{3}{2}) \leftrightarrow {}^4A_2(\pm\frac{1}{2})$  splitting is about  $0.1 \text{ cm}^{-1}$ , the former doublet being the lower in energy. The GSS for Na  $\beta$ -alumina should be similar to that of Ag  $\beta$ -alumina because the luminescence of the  $\text{Cr}^{3+}$  ion in the Al(4) site is not very sensitive to the nature of the mobile cation.<sup>10</sup> In fact, these ions occupy sites in the conduction planes which are relatively far from the Al(4) site ( $\sim 5.62 \text{ \AA}$ ).

The luminescence with the shorter lifetime [Fig. 4(a)] is characterized by a lower crystal field, a smaller sideband over the ZPL intensity ratio ( $R$ ), and a larger inhomogeneous linewidth. These facts lead one to assign this luminescence to  $\text{Cr}^{3+}$  ions in the octahedral Al(1) sites.<sup>9</sup> In fact, these sites are expected to present a crystal field lower than that of the Al(4) site because of the higher O–Al average distance [the average Al(1)–O distance is  $1.917 \text{ \AA}$ , while Al(4) site has 6 equidistant O ligands at  $1.895 \text{ \AA}$ ].<sup>32</sup> Furthermore, shorter lifetimes and smaller  $R$  values are consistent with the ED character of the transition which is allowed by presence of odd components of the crystal field at the Al(1) site, which has the low-symmetry  $C_s$ .

The nearness of the Al(1) site to the mirror plane, with its defective structure, causes rather large site-to-site fluctuations in the crystal-field parameters. As a consequence, even after selective excitation in energy, a single exponential decay is not observed and a nearly continuous distribution of lifetimes in the range 1–3 ms appears. Moreover, a quite large spread of the  $R_2$ – $R_1$  splitting is observed, which varies from 130 to  $160 \text{ cm}^{-1}$ , thus indicating a poor site-to-site correlation. The observed value for the GSS, taken at the maximum of the inhomogeneous line shape, is about  $1.2 \text{ cm}^{-1}$ .

The same kind of measurements were performed on intentionally  $\text{Cr}^{3+}$ -doped Na  $\beta$ -alumina crystals, grown in our laboratory with 5000 ppm of  $\text{Cr}^{3+}$  ions. Two different decay time regimes were still observed. As shown in Fig. 8, the centers characterized by a longer lifetime show a spectrum very similar to that of the not intentionally doped samples. However, some significant differences are present: the ZPL linewidth is larger [ $\Gamma_{\text{FWHM}} = 50 \text{ cm}^{-1}$  in Fig. 8(b) versus  $\Gamma_{\text{FWHM}} = 40 \text{ cm}^{-1}$  of Fig. 8(a)]; the ratio  $I_{\text{SB}}/I_{\text{ZPL}}$  is smaller ( $R=2$  versus

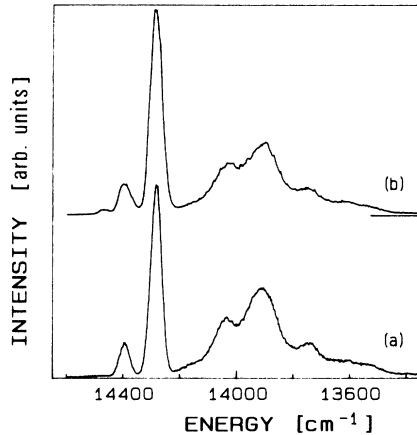


FIG. 8. Time-resolved luminescence spectra recorded at 77 K in (a) undoped Na  $\beta$ -alumina and (b) 5000-ppm  $\text{Cr}^{3+}$ -doped Na  $\beta$ -alumina, under excitation at 514.5 nm. The emitted light was analyzed with E1c and H1a. Pulse duration 50 ms and detection from 30 to 60 ms after laser switchoff.

$R=3$ ). Moreover, a shoulder appears at the highest-energy side and at least two distinct lifetimes are recorded ( $\tau_1=50$  ms and  $\tau_2=40$  ms versus the single lifetime  $\tau=70$  ms in the undoped compound); the shorter one is related to the shoulder structure at the high energy of the more intense ZPL. These results clearly reveal a more disordered structure with an average stronger distortion of the Al(4) site. This should be due to the defects present in the spinel block, induced by the  $\text{Cr}^{3+}$  content with possible pair effects, although we cannot rule out that they are related to a different sodium content.

### C. Sodium $\beta''$ -alumina, Mg stabilized

As for the case of  $\beta$ -alumina, the luminescence of  $\text{Cr}^{3+}$  ions substituting for  $\text{Al}^{3+}$  ions in the middle of the spinel block [site Al(1) in  $\beta''$ -alumina] can be isolated in the large delay time-resolved spectra [Fig. 3(b)]. By excitation in the homogeneously broadened  ${}^4A_2$ - ${}^4T_2$  band,  $\text{Cr}^{3+}$  ions at all sites can absorb, so that the inhomogeneous profile of the low-temperature luminescence gives a good measure of the site-to-site energy distribution of the  $R_1$  line. However, this is not exactly true because all the parameters affecting the luminescence are site dependent: absorption coefficients and line shapes in the  ${}^4A_2$ - ${}^4T_2$  transition, lifetimes and ZPL/SB ratios in the  ${}^2E$ - ${}^4A_2$  luminescence, and possibly quantum yields. In particular, the shape of the luminescence spectrum depends on the excitation frequency and on the detection delay after the laser pulse even for delays larger than 20 ms.

The three-peaked inhomogeneous profile of the  $R_1$  line extends over a range of about  $300\text{ cm}^{-1}$  and there is not a sharp separation between ZPL's and SB's. The shape of the sideband can be obtained by a FLN measurement, as reported in Fig. 9(a), by exciting in the low-energy tail of the  $R_1$  three-peaked luminescence in order to reduce other effects which complicate the spectrum, such as excitation of the  $R_2$  line. In Fig. 9(c), the contribution to the sideband is estimated by convoluting the SB shape of Fig. 9(a) with a ZPL line shape, approximated with three

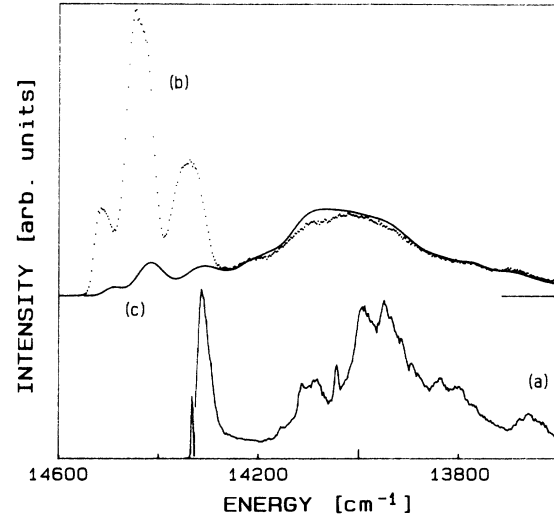


FIG. 9. Time-resolved luminescence spectra recorded at 4.2 K from long-living centers in  $\beta''$ -alumina, Mg-stabilized: (a) sideband spectrum obtained in the low-energy tail of the three-peaked  $R_1$  transition at  $14330\text{ cm}^{-1}$ . The ZPL has been filtered, its intensity being about 0.7 times the integrated intensity of the SB. Pulse width 40 ms and detection from 25 to 70 ms after laser switchoff; (b) spectrum of Fig. 3(b); (c) estimated contribution of the sideband (see text).

Gaussians. The SB line shape for  $\nu_0 < 14250\text{ cm}^{-1}$  is very well reproduced in the crude model which assumes the same  $R = I_{\text{SB}}/I_{\text{ZPL}} = 1.5$  ratio for all the centers. Moreover, it results that relevant SB contributions are also present in the region of  $R_1$  emission, due to the presence of the strong structure in the SB at low energy ( $\Delta E \approx 30\text{ cm}^{-1}$ ). The nature of this structure will be discussed elsewhere.

Figure 10 shows the time-resolved luminescence spectra obtained by exciting with a narrow band laser within the inhomogeneous profile [Fig. 10(a)]. Site selection is achieved, but the spectra are rather intriguing because three different sets of  $\text{Cr}^{3+}$  ions can be excited by pumping in the  $R_1$  line, in the  $R_2$  line, or in their sidebands. The first set of centers, which are excited in the  $R_1$  line, will luminesce in a sharp resonant line ( $R_1$ ) and the related sideband. In the low-temperature spectra, when the homogeneous linewidth is negligible, the width of the line is limited by the experimental resolution: the line is very sharp and intense so that it is plotted in the figure with an intensity reduced by a factor 20. The second set of centers, which are excited in the  $R_2$  line, after relaxation to the lower doublet of the  ${}^2E$  state, will luminesce at lower energy in the  $R_1$  line and its sideband. Finally, the third set of centers, which are excited in the sidebands relative to  $R_1$  or  $R_2$  line, will luminescence in their  $R_1$  line or sideband, giving rise to broad, poorly structured bands. The peaks of Figs. 10(b)–10(i), apart for the resonant ones, indicated by the arrows, correspond to  $R_1$  luminescence after excitation in the  $R_2$  line. A continuous distribution of  $R_1$ - $R_2$  splittings is not present: several rather narrow bands appear. This indicates the



presence of some sets of  $\text{Cr}^{3+}$  sites, which should be related to different structural defects in the nearest neighbors. Each set has rather well-defined values of the lifetimes and of the  $R_1$ - $R_2$  splittings, and appears for excitation just in limited energy ranges. It is possible to follow their behavior by comparing many spectra taken at different near excitation frequencies: the contribution of each set grows and decays with a nearly Gaussian shape, so that it is possible to localize peak energies and inhomogeneous linewidths. For instance, the set labeled *A* gives a contribution to Figs. 10(f)–10(i) with a nearly constant  $R_1$ - $R_2$  splitting of  $111\text{ cm}^{-1}$ . Actually the mean splitting slightly increases from  $108\text{ cm}^{-1}$  in Fig. 10(f) to  $113\text{ cm}^{-1}$  in Fig. 10(i). The analysis allows one to define an *A* set with a  ${}^2E$  splitting of  $111\text{ cm}^{-1}$ , a lifetime of 40–65 ms, with the  $R_1$  line centered at  $14\,334\text{ cm}^{-1}$ , and a distorted Gaussian shape with  $\text{FWHM}=65\text{ cm}^{-1}$ , having a long tail toward the low-frequency region.

The sharpness of most lines in the FLN spectra of Fig. 10 is due to a low residual inhomogeneous broadening:

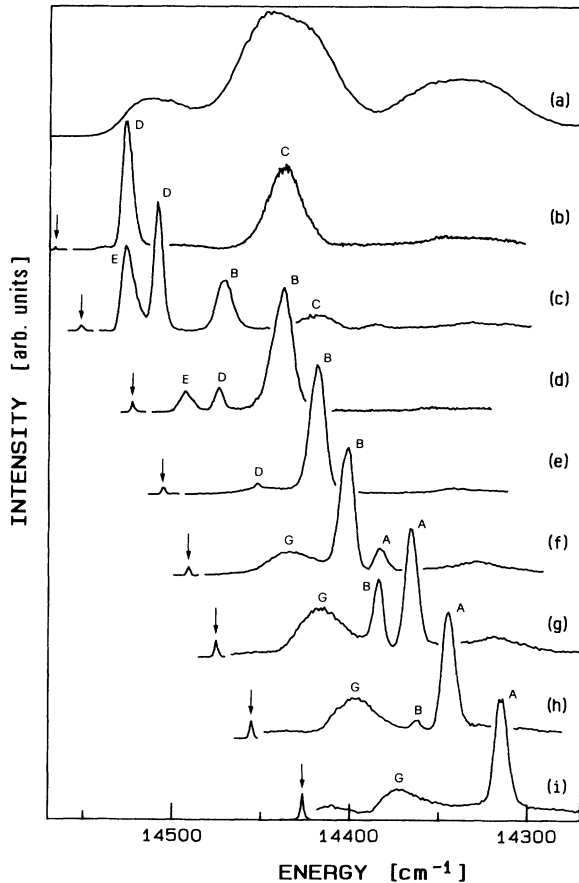


FIG. 10. Time-resolved luminescence spectra of  $\text{Cr}^{3+}$  ions in Na  $\beta'$ -alumina obtained at 4.2 K: (a) inhomogeneous profile of the three-peaked ZPL emission obtained under excitation of the 514.5-nm line; (b)–(i) are the FLN spectra under excitations at energies within the inhomogeneous profile, shown by the arrows. The intensities of the resonant ZPL are reduced by a factor 20. Labels refer to different sets of centers (see text). Pulse width 40 ms and detection from 25 to 70 ms after laser switchoff.

within a particular set of similar sites the  ${}^2E$  splitting is less sensitive to crystal-field fluctuations than the  $R_1$  and  $R_2$  energies themselves. In the case of set *A*, for instance, the residual inhomogeneous linewidth is about  $9\text{ cm}^{-1}$ , the  $R_1$  and  $R_2$  inhomogeneous linewidth being about  $65\text{ cm}^{-1}$ . The *C* and *G* sets have a different behavior: in fact, the residual linewidth is comparable to the  $R_1$  and  $R_2$  linewidths.

A similar study was performed by exciting with a pulsed dye laser in order to enhance the luminescence from centers Al(4) with short lifetimes. Some spectra are reported in Fig. 11 together with the inhomogeneous profile of Fig. 4. The features of these spectra appear much broader than those of Fig. 10 and a detailed analysis in terms of different sites is not possible. With the label *L* we group the overall contribution to the broadband peak at  $14\,300\text{ cm}^{-1}$ , whose internal structure is not resolved. Only two well-defined sites, labeled by *H* and *I*, are isolated by exciting in the high-energy tails of the inhomogeneous line shape as it results from the spectra of Figs. 11(b)–11(d). Lifetimes and  $R_1$ - $R_2$  splittings

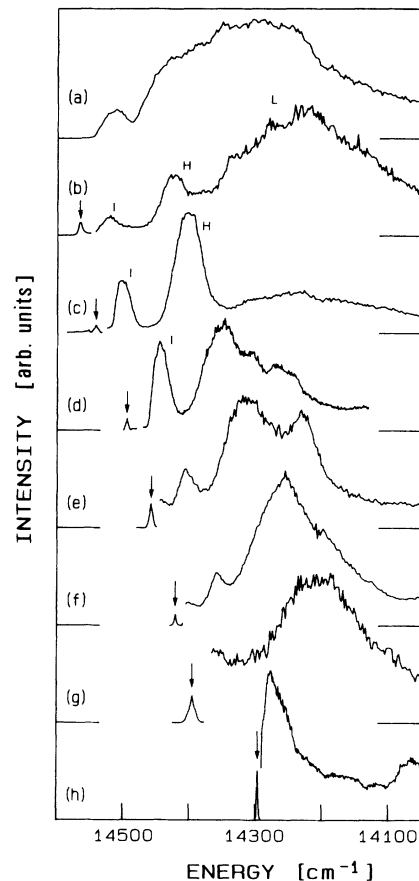


FIG. 11. Time-resolved luminescence spectra of  $\text{Cr}^{3+}$  ions in Na  $\beta'$ -alumina obtained at 4.2 K: (a) inhomogeneous profile of the ZPL emission obtained under excitation of the 514.5-nm line; (b)–(h) are the FLN spectra under laser excitations at energies within the inhomogeneous profile, shown by the arrows. The intensities of the resonant ZPL are reduced by a factor 100. Labels refer to different sets of centers (see text). Pulse width 20 ns and detection from 0.2 to 1.7 ms.

for the most relevant contribute to the luminescence seems to show a continuous distribution of centers. For laser energies lower than  $14\,300\text{ cm}^{-1}$ , as in Fig. 11(h), only centers in the  $R_1$  line are excited so that the SB shape is the only nonresonant contribution. It should be noted that the spectra of Figs. 10 and 11 are normalized to their maximum for graphical reasons, so the intensity behavior is not directly observable. The relevant occurrence of  $\text{Cr}^{3+}$  ions in the different sites can, however, be obtained from the observed intensities. The latter, however, strongly depend on the experimental conditions as evidenced in Fig. 12, where the spectra obtained with different time intervals of excitation and detection for excitation at a fixed energy are compared. The use of both pulsed and cw laser sources is indeed essential in order to have even a rough estimate of the relative contributions from centers with different lifetimes. The relative occurrence was obtained from the rate equations, knowing the lifetime and assuming the following hypotheses: (i) the quantum yield is equal to 1; (ii) the emission in the SB has the same probability for any  $\text{Cr}^{3+}$ : parity mixing induced by odd vibrations is assumed to be site independent; (iii) the ratio of absorption rate in  $R_1$  and  $R_2$  lines is site independent. We estimate a typical error of 50% for the obtained values, but possible systematic errors due to the simplifying assumptions cannot be excluded.

Figures 13 and 14 show the luminescence spectra obtained with higher resolution in the range across the excitation laser line. The ground state  ${}^4A_2$  is split in two doublets ( $m_s = \pm\frac{3}{2}, \pm\frac{1}{2}$ ) for any crystal field of symmetry lower than octahedral. Therefore, the  $R_1$  line of each center is also split in two lines ( $R_{1a}, R_{1b}$ ). Site selection

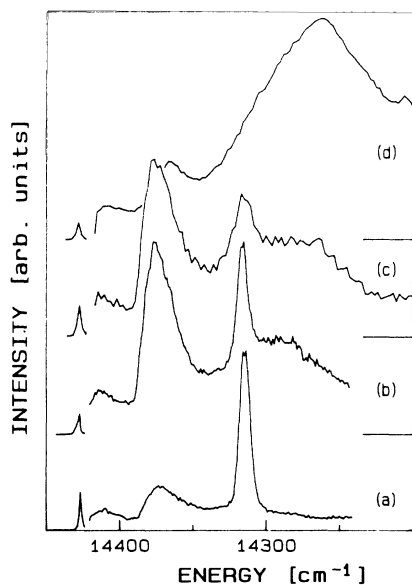


FIG. 12. Time-resolved luminescence spectra of  $\text{Cr}^{3+}$  ions in Na  $\beta'$ -alumina obtained at 4.2 K by exciting at  $14\,428\text{ cm}^{-1}$  with different laser sources: (a) and (b) with a cw laser, mechanically chopped (40-ms pulse width); and (c) and (d) with a pulsed laser (20-ns pulse width). The detection windows are (a) from 25 to 70 ms after laser switchoff; (b) from 17 to 29 ms; (c) from 17 to 31 ms; and (d) from 0.2 to 1.7 ms.

is achieved for two groups of ions, those having the  $R_{1a}$  or  $R_{1b}$  resonant with the narrow laser line, respectively. Each group will, in turn, luminescence from the  ${}^2E$  lower doublet in the two lines producing a three-peaked spectrum. The central peak correspond to resonant  $R_{1a}$  ( $R_{1b}$ ) luminescence after excitation in  $R_{1a}$  ( $R_{1b}$ ). It is very sharp at low temperature and actually its line shape in Figs. 13 and 14 is due to the experimental setup. The bands on the two sides of the central peak correspond to absorption in  $R_{1a}$  and luminescence in  $R_{1b}$  or vice versa: their shape reflects the distribution of ground-state splittings. The thermal population ratio of the two  ${}^4A_2$  doublets regulates the intensity ratio of the bands on the two sides. At 4.2 K for  ${}^4A_2$  splittings  $\Delta E \geq 1\text{ cm}^{-1}$ , the thermal populations of the two doublets are appreciably different as it appears in Figs. 13(e) and 13(f) and in Fig. 14. The spectra are not corrected for the spectrometer response which is asymmetric. The apparent higher intensity of the higher-energy component in Fig. 13(a) is a spurious effect. Wide distributions of ground-state splittings are evident from Fig. 13, which is relative to the long-living centers. As for  ${}^2E$ , there is not a continuous distribution of splittings, but different sets of  $\text{Cr}^{3+}$  ions with rather defined ground-state splittings appear at any

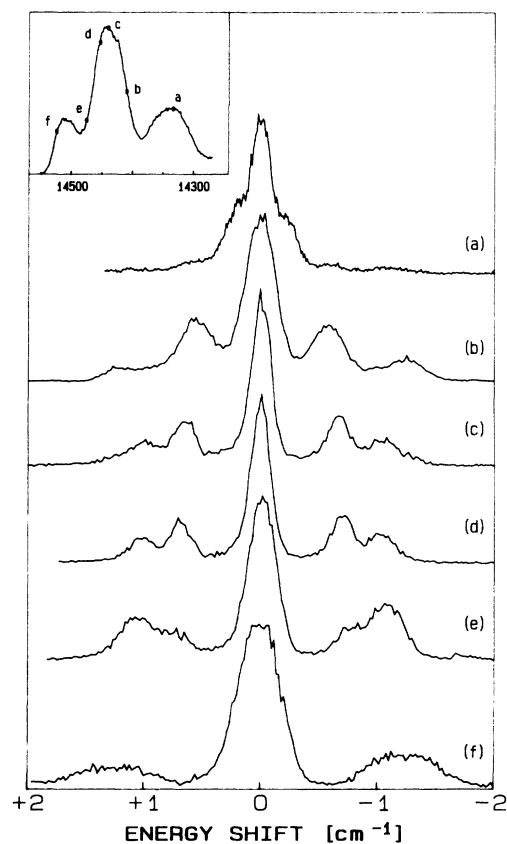


FIG. 13. FLN spectra of the  ${}^2E$ - ${}^4A_2$  transition of  $\text{Cr}^{3+}$  ions in Al(1) sites of Na  $\beta'$ -alumina crystal at 4.2 K for six different excitation energies within the inhomogeneous profile as shown in the inset: (a)  $14\,358\text{ cm}^{-1}$ ; (b)  $14\,474\text{ cm}^{-1}$ ; (c)  $14\,456\text{ cm}^{-1}$ ; (d)  $14\,425\text{ cm}^{-1}$ ; (e)  $14\,413\text{ cm}^{-1}$ ; and (f)  $14\,330\text{ cm}^{-1}$ . Pulse width 40 ms, detection from 30 to 80 ms after laser switchoff.

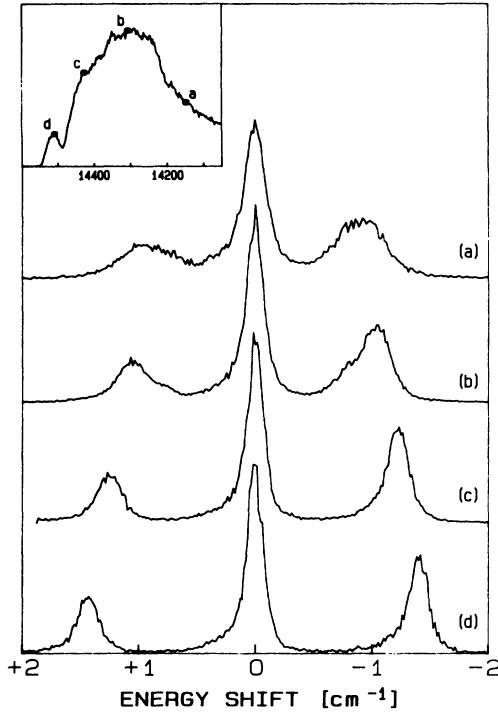


FIG. 14. FLN spectra of the  ${}^2E$ - ${}^4A_2$  transition of  $\text{Cr}^{3+}$  ions in Al(4) sites of Na  $\beta'$ -alumina crystal at 4.2 K for four different excitation energies within the inhomogeneous profile as shown in the inset: (a) 14 150  $\text{cm}^{-1}$ ; (b) 14 300  $\text{cm}^{-1}$ ; (c) 14 423  $\text{cm}^{-1}$ ; and (d) 14 505  $\text{cm}^{-1}$ . Pulse width 20 ns and detection from 0.2 to 1.7 ms.

excitation frequency. By comparing lifetimes and spectra obtained at different excitation energies in the range of  $R_1$  occurrence, it was possible in most cases to relate the data relative to  ${}^4A_2$  and  ${}^2E$  states. For the short-living centers of Fig. 14, once again as for the case of the  ${}^2E$  state, it does not appear a discrete number of sets of centers with well-defined ground-state splittings. A con-

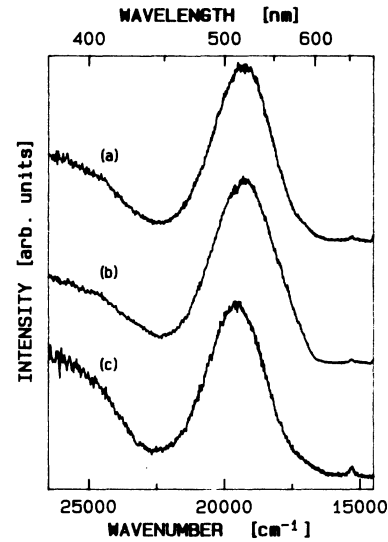


FIG. 15. Time-resolved excitation spectra recorded at 77 K in Na  $\beta'$ -alumina:  $\text{Cr}^{3+}$ . Pulse duration 60 ms and detection from 20 to 70 ms after laser switchoff. The emission is observed at (a) 14 508  $\text{cm}^{-1}$ , (b) at 14 445  $\text{cm}^{-1}$ , and (c) at 14 320  $\text{cm}^{-1}$ , the energies of three peaks of Fig. 3(b).

tinuous distribution of splittings from about 0.6 to 1.2  $\text{cm}^{-1}$  is observed in Figs. 14(a) and 14(b). The mean splitting increases by increasing the  $R_1$  energy. In the high-energy tail of the  $R_1$  inhomogeneous profile, the ground-state splitting is very well defined, as it appears from the sharp peak in Figs. 13(c) and 13(d). It is indeed possible to assign a GSS of 1.2  $\text{cm}^{-1}$  to set I, which originates the peaked luminescence centered at 14 505  $\text{cm}^{-1}$  in the inset of Fig. 14. The data relative to the different sets of  $\text{Cr}^{3+}$  ions, which we were able to isolate by means of the present analysis, are resumed in Table II.

It was not possible to select for each set of centers of Table II, the excitation spectrum, which would give the

TABLE II. Characteristic parameters of  $\text{Cr}^{3+}$ -ion luminescence in  $\beta$ - and  $\beta'$ -alumina at 4.2 K. For each set of sites, whose contributions were isolated, we report the energy position ( $\text{cm}^{-1}$ ) of the  $R_1$  line, its inhomogeneous linewidth ( $\text{cm}^{-1}$ ), its residual inhomogeneous linewidth ( $\text{cm}^{-1}$ ), i.e., the  $R_1$  linewidth after narrowband excitation in its  $R_2$  counterpart, the  ${}^2E$  and  ${}^4A_2$  splittings ( $\text{cm}^{-1}$ ), the lifetimes, and the relative occurrence estimated on the basis of the observed intensities.

	Site	$R_1$	$R_2-R_1$	FWHM inhom.	FWHM resid.	${}^4A_2$ split.	$\tau$ (ms)	Relative occurrence
Na $\beta'$	A	14 334	111	65	9	0.2	40–65	1
	B	14 431	84	50	12	1	30	1
	C	14 454	128	35	20	0.7	25–30	0.2
	D	14 503	44	35	7		35	0.2
	D	14 521	25	20	10	1.2	20	0.1
	F	14 365	60	44	30	1	4–6	1
	G	14 420	60	33	27	1.15	8–10	0.2
	H	14 395	50	46	40	1.4	5	
	I	14 505	40	30	28	1.2	3	
	L	14 300	130–150	> 100		0.6–1.2	1.5–3	~25
Na $\beta$	Al(4)	14 265	113	40	15	< 0.2	70	
	Al(1)	14 130	150	100	60	1.2	1.7	

energy position of the  ${}^4T_2$  and  ${}^4T_1$  levels. In Fig. 15 we report the time-resolved excitation spectra taken on the maxima of the three-peaked long-lifetime luminescence. The spectra indicate that the crystal fields are very similar ( $Dq \simeq 1930 \text{ cm}^{-1}$ ) and show a small shift towards low energy of the  ${}^4A_2$ - ${}^4T_2$  broadband as the  ${}^2E$ - ${}^4A_2$  detection energy is increased. Therefore, the centers which luminesce at higher energy are characterized by a lower crystal field. The energy of the small structure due to the  ${}^4A_2 \rightarrow {}^2T_1$  transition does not change appreciably. As for the luminescence with a shorter lifetime, i.e., sites *L*, a lower value of the crystal field is observed ( $Dq \simeq 1720 \text{ cm}^{-1}$ ).

## V. DISCUSSION

Let us focus our attention on the luminescence relative to  $\text{Cr}^{3+}$  ions in the site at the center of the spinel block. In sodium  $\beta$ -alumina a single set of  $\text{Cr}^{3+}$  ions, following the classification procedures of Table II, is observed: lifetimes,  ${}^2E$  and  ${}^4A_2$  splittings were similar for all the centers. A nondefect crystalline surrounding for  $\text{Cr}^{3+}$  ions was deduced and inhomogeneities were ascribed to the disordered structure of the conduction planes which cause relatively small site-to-site fluctuations of the crystal field at the Al(4) site for  $\text{Cr}^{3+}$ .

The data of Table II suggest a more complex situation for  $\beta'$ -alumina. The centers with long lifetimes ( $\tau > 20$  ms), i.e., sets *A*–*E*, have to be ascribed to  $\text{Cr}^{3+}$  ions in the Al(1) site, which correspond to the Al(4) site in  $\beta$ -alumina. The centers *L*, with lifetimes of the order of 1–3 ms, should be assigned to the Al(4) site. Sites *F*–*I*, which present intermediate lifetimes, will be considered later. Therefore, in  $\beta'$ -alumina we are faced with at least five different, quite well-defined, sets of  $\text{Cr}^{3+}$  in Al(1) site. This fact can be understood if we consider that in  $\beta'$ -alumina, in addition to the disorder of the  $\text{Na}^+$ -ion sublattice, a defect structure is expected in the spinel block due to the replacement of some  $\text{Al}^{3+}$  by  $\text{Mg}^{2+}$  ions. One is indeed led to find a simple correlation between the different sets of Table II and the discrete number of  $\text{Mg}^{2+}$  configurations in the neighbors of  $\text{Cr}^{3+}$  ions, which should produce rather well-defined energy level sequences and transition probabilities. The disorder of the defective structure of  $\text{Na}^+$  ions in the conduction region should add a distribution of fields which produces a line broadening, as for the case of  $\beta$ -alumina.

By assuming the nominal composition  $\text{Na}_{1.67}\text{Mg}_{0.67}\text{Al}_{10.33}\text{O}_{17}$  for  $\beta'$ -alumina, it would result that two of 33  $\text{Al}^{3+}$  ions in the unit cell are substituted for  $\text{Mg}^{2+}$  ions, originating a defect with net negative charge which stabilizes the mean concentration of 5  $\text{Na}^+$  ions in the three conduction planes of the unit cell. From neutron-diffraction measurements it results that the replacement preferentially occurs in the site Al(2) with a much smaller occupation of the other tetrahedral site Al(4).<sup>13</sup> The simplest model can indeed assume that, on the average, two of the sixth nearest Al(2) around the Al(1) sites in  $\beta'$ -alumina are occupied by  $\text{Mg}^{2+}$  ions. Table III gives a schematic representation of the possible nonequivalent configurations with 0, 1, 2  $\text{Mg}^{2+}$  ions. The

Al(1)–Al(2) site separation is about  $3.29 \text{ \AA}$ . The six Al(2) sites are displaced by about  $\pm 0.57 \text{ \AA}$  along the crystallography *c* axis, with respect to the plane containing the Al(1) sites, in an alternate way. The net negative charge associated to a  $\text{Mg}^{2+}$  ion will produce an electric field at the Al(1) site with a relative stronger component perpendicular to the *c* axis ( $E_{\perp c}$ ) and a weaker parallel one ( $E_{\parallel c}$ ). A simple point-charge model, without lattice relaxation, gives the electric field reported in Table III for the different configurations in units of the field ( $E_{\perp c}$ ) generated by the replacement of a single  $\text{Mg}^{2+}$  ion. The probabilities of occurrence reported there are calculated by assuming random distributions of the  $\text{Mg}^{2+}$  ions in the Al(2) sites with a probability value  $\frac{1}{3}$ . The following effects are expected.

(i) The electric field will cause an odd distortion which removes the inversion symmetry and by parity mixing allows the ED transition, with a shortening of the lifetime.

(ii) The substitution in the Al(2) site of a  $\text{Mg}^{2+}$  ion should modify the crystal field at the Al(1) site because of the different charge and the bigger ionic radius ( $0.72 \text{ \AA}$  for the  $\text{Mg}^{2+}$  ion,  $0.5 \text{ \AA}$  for the  $\text{Al}^{3+}$  ion<sup>9</sup>). This fact should also vary the crystal-field parameter *Dq* which determines the energy position of the  ${}^4A_2$ - ${}^4T_2$  band. Moreover, a lowering of the crystal-field symmetry from the  $D_{3d}$  one should influence both the GSS and the  ${}^2E$  splitting. On the basis of the above considerations, we can now try to correlate the centers *A*–*E* to the different configurations depicted in Table III. The set *A* presents spectroscopic properties (lifetime, energy of  ${}^2E$ , ground state, and  ${}^2E$  splittings) which are closest to those of the site Al(4) in  $\beta$ -alumina and therefore it is assigned to the configuration without  $\text{Mg}^{2+}$  ions. The lifetime and relative occurrence induced to assign the *B* luminescence to the site with one  $\text{Mg}^{2+}$  around, the *C*, *D*, and *E* luminescences to sites with two  $\text{Mg}^{2+}$  ions around. Among these, the emission *E* with the shortest lifetime should correspond to the last configuration which shows the strongest odd-parity electric field and the emission *D*, with longer lifetime, to the third configuration which is symmetrical. We would like to find a confirmation of the above assignments, based on the lifetimes, from the other spectroscopic properties, i.e., energy positions and splittings of the levels. The energy position of the baricenter of the  ${}^2E$  level,  $(E_{R1} + E_{R2})/2$ , shifts to higher energies passing from the center *A* to *B* and to *C*, *D*, *E*. At the same time the  ${}^4A_2$ - ${}^4T_2$  transition shifts to lower energies, as shown by the excitation spectra of Fig. 15. From the Tanabe and Sugano diagrams<sup>33</sup> one expects a weak increase of the energy of the  ${}^2E$  state as the crystal field increases: the s.o. interaction between the  ${}^2E$  and  ${}^4T_2$  states mainly governs this behavior. The opposite behavior in  $\beta$ -aluminas indicates that the low symmetry field contributions dominate on the s.o. coupling in affecting the energy position of the  ${}^2E$  state. As for the  ${}^2E$  and  ${}^4A_2$  splittings, no systematic trend is observed. On the other hand, it is well known that an accurate estimation of these splittings is possible only in few cases even in well-defined symmetry as trigonal or tetragonal.<sup>24,25,34,35</sup>

At the present time, the evaluation of the splittings for

the low symmetry configurations of Table III does not seem to be possible. In fact, the symmetry of the site becomes very low when the distortions are summed to the trigonal one along the  $c$  axis. Moreover, it should be noticed that the signs of the splittings of the centers of Table II are known only for the Al(4) site in  $\beta$ -alumina. Finally, one should also note that the residual disorder of the structure does not have the same effect on the various sets, as it results from the quite different FWHM's.

There is not a close correlation between the relative occurrence of the  $A-E$  centers and the distribution of probabilities (Table II) calculated on the assumption of a random distribution of two  $\text{Mg}^{2+}$  ions in the unit cell. It is possible that some correlations Mg-Mg and Mg-Cr exist. However, we notice that, still assuming a random occupation of the available sites, a better agreement would be obtained with a lower content of  $\text{Mg}^{2+}$  ions, for instance, 1.5  $\text{Mg}^{2+}$  ions in the unit cell. On the other hand, we observe other relatively intense contributions to the luminescence, sets  $F$  and  $G$ , which seem to be related to  $\text{Cr}^{3+}$  ions in strongly distorted Al(1) sites rather than in Al(4) ones, mainly on the basis of their lifetimes. It is possible that other defects, such as  $\text{Al}^{3+}$  vacancies, give a relevant contribution to the charge stabilization in com-

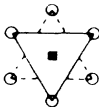
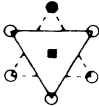
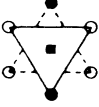
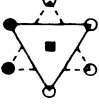
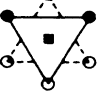
petition with that of the stabilizing  $\text{Mg}^{2+}$  ions. Such defects should strongly affect the crystal field acting on the  $\text{Cr}^{3+}$  ion in the Al(1) site and should produce effects on its spectroscopic properties like those observed for the sets  $F$  and  $G$ : a well-defined crystal-field parameter with strong distortion from the original trigonal symmetry, which produces, in turn, relatively sharp lines with short lifetimes.

The intense luminescence  $L$ , and possibly the luminescences  $H$  and  $I$ , have to be assigned to  $\text{Cr}^{3+}$  ions in Al(4) sites due to their lower lifetimes and higher sensitivity to the disorder. In fact, the lifetime and the splittings of both ground and excited states of set  $L$  are very similar to those of  $\text{Cr}^{3+}$  in the Al(1) site of  $\beta$ -alumina. The strong effect of the  $\text{Na}^+$  disordered distribution on such luminescence prevents a more detailed analysis and a clear identification of different sets as for the  $A-G$  centers.

## VI. CONCLUSIONS

A detailed analysis of the luminescence of  $\beta''$ -alumina shows properties which are typical of the particular disordered structure. Two kinds of defects which have

TABLE III. Schematic representation of unequivalent local arrangements for  $\text{Mg}^{2+}$  ions around the  $\text{Cr}^{3+}$  ion at the Al(1) site in Na  $\beta''$ -alumina.  $E_{\perp c}$  and  $E_{\parallel c}$  are the components of the electric field  $E$  (in units of  $E_{\parallel c}$ ) at the  $\text{Cr}^{3+}$  site perpendicular and parallel to the crystallographic  $c$  axis, respectively.  $P$  gives the probability of the different configurations for specific  $\text{Mg}^{2+}$ -ion content per unit cell (see text). Finally, the last column gives a tentative correlation between the different configurations and the sets of Table II.

Configuration	$E_{\perp c}$	$E_{\parallel c}$	$ E $	P(1/3)%	P(1/4)%	Set
	0	0	0	8.8	17.8	A
	1	.18	1.016	26.3	35.6	B
	0	0	0	6.6	5.9	D
	$\sqrt{3}$	0	1.73	13.2	11.8	C
	1	.35	1.06	13.2	11.8	E

different effects on the luminescence can be identified. The  $\text{Na}^+$  ions' distribution in the conduction regions acts as a random strain, which broadens the lines to a nearly Gaussian line shape and gives rise to a distribution of the other parameters as lifetimes and splittings. On the contrary, the defects due to  $\text{Mg}^{2+}$  substitutional for  $\text{Al}^{3+}$  ions give a relatively well-defined crystal-field perturbation.

By means of FLN measurements, different sets of centers with characteristic luminescence parameters can be isolated. Even if a close correlation between the observed luminescences and the expected configurations of defective  $\text{Mg}^{2+}$  ions is not always found, the defective structure of the system is well evidenced. The presence of centers with strong crystal-field distortion suggest the presence of other charge compensation mechanisms as such  $\text{Al}^{3+}$  vacancies.

The complex structure of the luminescence has relevant consequences on the study of the temperature dependence of the homogeneous linewidth. In fact, the homogeneous linewidth is site dependent, so that the line shape can be fitted by a single Lorentzian curve only when the contribution to the luminescence from a single set of sites is isolated. In general, the actual line shape contains contributions of various sites, and in some cases, as shown in Fig. 4 of Ref. 36, the nearly equivalent con-

tributions can be isolated by fitting the line shape with two Lorentzian curves. Detailed results will be presented elsewhere, but we want to stress here the particular difficulty that we have found in this study. In order to study the evolution of the linewidth with temperature one should select by FLN a particular set of centers and maintain it under observation when raising the temperature. This is not so easy, in general, because all the parameters which identify the different sites, as the energy transitions and lifetimes, are continuously varying with temperature. In this way it may happen that the observed luminescence comes from a set of sites continuously changing with temperature and so the temperature dependence of the linewidth loses an important part of its physical meaning. Such a difficulty, while in this system is well evidenced due to the coexistence of different sets of sites with rather well-defined parameters, is even harder to overcome in fully disordered systems.

#### ACKNOWLEDGMENTS

The authors are grateful to Professor G. C. Farrington for kindly providing them with the samples. They also like to thank V. Cavecchia, F. Gottardi, and F. Berti of their skillful technical support. Finally, the financial support by the Consiglio Nazionale delle Ricerche, under Contract No. 88.01726.02, is gratefully acknowledged.

- <sup>1</sup>J. L. Sudworth and A. R. Tilley, *The Sodium Sulfur Battery* (Chapman and Hall, London, 1985).
- <sup>2</sup>G. C. Farrington, B. Dunn, and J. O. Thomas, *Appl. Phys. A* **32**, 159 (1983).
- <sup>3</sup>S. Sattar, G. Ghosal, M. L. Underwood, H. Mertwoy, M. A. Saltzberg, W. S. Frydrych, G. S. Rohrer, and G. C. Farrington, *J. Solid State Chem.* **65**, 231 (1986).
- <sup>4</sup>M. Jansen, A. Alfrey, O. M. Stafsudd, B. Dunn, D. L. Yang, and G. C. Farrington, *Opt. Lett.* **9**, 119 (1984).
- <sup>5</sup>R. W. Boyd, M. T. Gruneisen, P. Narum, D. J. Simkin, B. Dunn, and D. L. Yang, *Opt. Lett.* **11**, 162 (1986).
- <sup>6</sup>J. D. Barrie, B. Dunn, O. M. Stafsudd, and P. Nelson, *J. Lumin.* **37**, 303 (1987).
- <sup>7</sup>J. D. Barrie, B. Dunn, O. M. Stafsudd, and G. C. Farrington, *Solid State Ion.* **18&19**, 677 (1986).
- <sup>8</sup>R. C. Powell, G. E. Venikouas, L. Xi, and J. B. Bates, *J. Lumin.* **37**, 1 (1987).
- <sup>9</sup>G. Mariotto, M. Montagna, and F. Rossi, *J. Phys. C* **19**, 3029 (1986).
- <sup>10</sup>G. Mariotto, M. Montagna, and F. Rossi, *Phys. Rev. B* **38**, 1072 (1988).
- <sup>11</sup>P. V. Anderson, B. I. Halperin, and C. Varma, *Philos. Mag.* **25**, 1 (1972); W. A. Phillips, *J. Low Temp. Phys.* **7**, 351 (1972).
- <sup>12</sup>For a recent review, see U. Strom, *Key Eng. Mater.* **59&60**, 35 (1991).
- <sup>13</sup>M. Bettman and C. R. Peters, *J. Chem. Phys.* **73**, 1774 (1969).
- <sup>14</sup>C. R. Peters, M. Bettman, J. W. Moore, and M. D. Glick, *Acta Crystallogr. B* **27**, 1826 (1971).
- <sup>15</sup>M. S. Whittingham and R. A. Huggins, *J. Electrochem. Soc.* **118**, 1 (1971).
- <sup>16</sup>Y.-F. Yao and J. T. Kummer, *J. Inorg. Nucl. Chem.* **29**, 2453 (1967).
- <sup>17</sup>D. B. McWhan, P. D. Dernier, C. Vettier, A. S. Cooper, and J. P. Remeika, *Phys. Rev. B* **17**, 4043 (1978).
- <sup>18</sup>W. L. Roth, F. Reidinger, and S. LaPlaca, in *Superionic Conductors*, edited by G. D. Mahan and W. L. Roth (Plenum, New York, 1976), pp. 223–241.
- <sup>19</sup>J. D. Jorgensen, F. J. Rotella, and W. L. Roth, *Solid State Ion.* **5**, 143 (1981).
- <sup>20</sup>K. G. Frase, J. O. Thomas, and G. C. Farrington, *Solid State Ion.* **9/10**, 307 (1983).
- <sup>21</sup>J. L. Briant and G. C. Farrington, *J. Solid State Chem.* **33**, 385 (1980).
- <sup>22</sup>G. Mariotto, M. Montagna, F. Rossi, E. Zanghellini, and E. Cazzanelli, *Key Eng. Mater.* **59&60**, 77 (1991).
- <sup>23</sup>G. Mariotto, M. Montagna, and F. Rossi, *Solid State Ion.* **28-30**, 311 (1988).
- <sup>24</sup>R. M. McFarlane, *J. Chem. Phys.* **39**, 3118 (1963).
- <sup>25</sup>R. M. McFarlane, *J. Chem. Phys.* **47**, 2066 (1967).
- <sup>26</sup>Du Maolu and C. Rudowicz, *Phys. Rev. B* **46**, 8974 (1992).
- <sup>27</sup>C. D. Flint, A. P. Mattheus, and P. J. O'Grady, *J. Chem. Soc. Faraday Trans. II* **73**, 655 (1977).
- <sup>28</sup>C. D. Flint and A. P. Mattheus, *J. Chem. Soc. Faraday Trans. II* **76**, 1381 (1977).
- <sup>29</sup>D. F. Nelson and M. D. Sturge, *Phys. Rev.* **137**, A1117 (1965).
- <sup>30</sup>N. B. Manson and G. A. Shah, *J. Phys. C* **10**, 1991 (1977).
- <sup>31</sup>A. Monteil, *J. Phys. Condens. Matter* **2**, 9639 (1990).
- <sup>32</sup>J. P. Boilot, G. Collin, Ph. Colomban, and R. Comes, *Phys. Rev. B* **22**, 5912 (1980).
- <sup>33</sup>S. Sugano, Y. Tanabe, and H. Kamimura, in *Multiplets of Transition Metal Ions in Crystals* (Academic, New York, 1970).
- <sup>34</sup>C. D. Flint and A. P. Mattheus, *J. Chem. Soc. Faraday Trans. II* **70**, 1307 (1974).
- <sup>35</sup>C. D. Flint and A. P. Mattheus, *Inorg. Chem.* **14**, 1008 (1975).
- <sup>36</sup>T. Beltrame, G. Mariotto, M. Montagna, and F. Rossi, *J. Lumin.* **48&49**, 537 (1991).

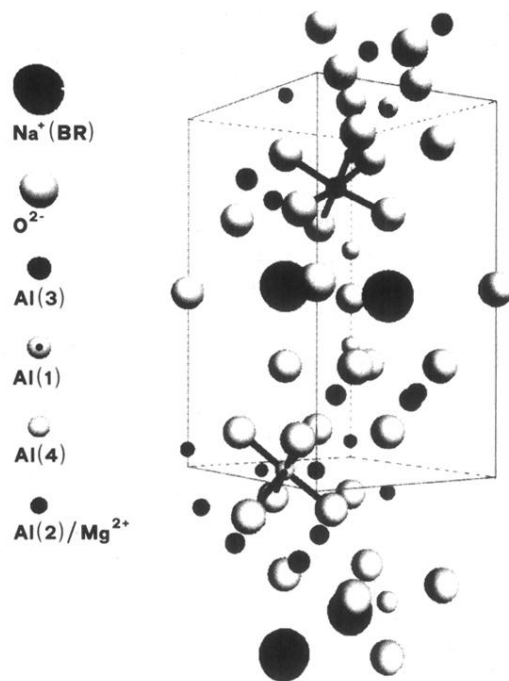


FIG. 1. Stereoscopic view of sodium  $\beta''$ -alumina structure, showing two half spinel blocks adjacent to the conduction plane region. The tetrahedral and octahedral sites of  $\text{Al}^{3+}$  ions within the spinel block are labeled according to Ref. 20. The ligands of the two octahedral sites are evidenced.  $\text{Na}^+$  ions are located in Beevers-Ross (BR) sites, but slightly displaced ( $\approx 0.17 \text{ \AA}$ ) out from the plane of the bridging oxygens O(5). Finally, the stabilizing  $\text{Mg}^{2+}$  ions are substitutional for  $\text{Al}^{3+}$  ions in Al(2) sites.